Nature of orbital and spin Rashba coupling in the surface bands of $SrTiO_3$ and $KTaO_3$

Panjin Kim, Kyeong Tae Kang, Gyungchoon Go, and Jung Hoon Han*
Department of Physics, Sungkyunkwan University, Suwon 440-746, Korea
(Received 1 May 2014; revised manuscript received 22 October 2014; published 18 November 2014)

Tight-binding models for the recently observed surface electronic bands of $SrTiO_3$ and $KTaO_3$ are analyzed with a view to bringing out the relevance of momentum-space chiral angular momentum structures of both orbital and spin characters. The orbital and the accompanying spin angular momentum structures reveal complex linear and cubic dependencies in the momentum **k** (linear and cubic Rashba effects, respectively) in a band-specific manner. Analytical expressions for the cubic orbital and spin Rashba effects are derived by way of a unitary transformation technique we developed, and compared to numerical calculations. The cubic Rashba effect appears as in-plane modulations due to the C_{4v} symmetry of the perovskite structure.

DOI: 10.1103/PhysRevB.90.205423 PACS number(s): 73.20.−r, 73.21.−b, 79.60.Jv

I. INTRODUCTION

The discovery of surface electronic states in strontium titanate ($SrTiO_3$) [1,2] has stirred great excitement and at this time the material is being regarded as a critical component in the emerging field of oxide electronics [3]. The origin of surface states in $SrTiO_3$ and a related material $KTaO_3$ [4,5] (STO and KTO for short, respectively) is currently under active investigation [5,6]. Both materials' surface states originate from t_{2g} orbitals whose relevant tight-binding parameters for the electronic structure are largely determined, including the one pertaining to the degree of inversion symmetry breaking (ISB) at the surface [5,6].

Several features make STO and KTO surface states an ideal ground for the study of Rashba-related phenomena. The first is the way that Rashba effects would play out among the several observed bands of differing orbital characters. At the moment ARPES measurements [1,2,4,5] are unable to resolve the Rashba-split bands clearly, presumably due to the smallness of the predicted Rashba parameter [7]. Transport measurement, on the other hand, do reveal the Rashba term of cubic order in momentum through analysis of the orientation-dependent magnetoresistance data on the STO surface [8,9]. Existing theories treat Rashba effects of t_{2g}-derived bands phenomenologically [6,10] and cannot, for instance, explain the complex band-specific spin and orbital angular momentum structures observed in the electronic structure calculation [7].

It was argued recently that multiorbital bands, subject to the surface ISB electric field, must give rise to an entity called the chiral orbital angular momentum (OAM) in momentum space [11,12]. The argument remains valid as long as the crystal field splitting does not quench the multiorbital degree of freedom in a given band structure. Such conditions seem to apply well in both STO and KTO, predicting a term $\sim \mathbf{k}\times\mathbf{E}\cdot\mathbf{L}$ where $\mathbf{L}$ is the OAM operator for t_{2g} orbitals, $\mathbf{k}$ is the linear momentum, and $\mathbf{E}$ is the surface-normal electric field. The effect was previously dubbed the "orbital Rashba effect" [11] in analogy to the similar chiral structure of spins on the surface [13]. It was further shown that the preexisting chiral OAM structure implies the linear Rashba effect upon the inclusion of spin-orbit interaction [11].

The ideas and techniques developed in Ref. [11] are now extended to address cubic-order Rashba effects, of both orbital and spin origins. The complex interplay of spin and orbital textures in momentum space can be understood in a systematic and band-specific manner through such analysis. Based on t_{2g}-orbital models pertinent to STO and KTO surfaces, we derive cubic orbital and spin Rashba terms consistent with the C_{4v} symmetry of the perovskite structure. Earlier derivation of the cubic Rashba term for the C_{3v}-symmetric single-band surface of topological insulators predicted the coupling of cubic momentum to the out-of-plane spin component [14]. The C_{4v} symmetry of the perovskite surface in contrast dictates cubic momentum dependence in the *in-plane modulation* of orbital and spin textures.

II. DERIVATION OF CHIRAL ORBITAL ANGULAR MOMENTUM BY UNITARY ROTATION

The tight-binding Hamiltonian we employ is analogous to the ones discussed in several papers [5,6,15,16]:

$$\mathcal{H} = \sum_{\mathbf{k},\sigma} \mathbf{C}^\dagger_{\mathbf{k},\sigma}\mathcal{H}_0\mathbf{C}_{\mathbf{k},\sigma} + \sum_{\mathbf{k}} \mathbf{C}^\dagger_{\mathbf{k}}\mathcal{H}_{\rm so}\mathbf{C}_{\mathbf{k}},$$

$$\mathcal{H}_0 = -\begin{pmatrix} 2t(c_x+c_y)-\delta & -2i\gamma s_x & -2i\gamma s_y \\ 2i\gamma s_x & 2tc_y+2t'c_x & 0 \\ 2i\gamma s_y & 0 & 2tc_x+2t'c_y \end{pmatrix},$$

$$\mathcal{H}_{\rm so} = \lambda_{\rm so}\mathbf{L}\cdot\boldsymbol{\sigma}. \quad (1)$$

The spin-orbit matrix $\mathcal{H}_{\rm so}$ in its explicit form can be found in Refs. [6,16]. The second-quantized operators are written in the basis ($\sigma = \uparrow,\downarrow$):

$$\mathbf{C}_{\mathbf{k},\sigma} = (c_{\mathbf{k},xy,\sigma}, c_{\mathbf{k},yz,\sigma}, c_{\mathbf{k},zx,\sigma})^{\mathsf{T}},$$

$$\mathbf{C}_{\mathbf{k}} = (c_{\mathbf{k},xy,\uparrow}, c_{\mathbf{k},xy,\downarrow}, c_{\mathbf{k},yz,\uparrow}, c_{\mathbf{k},yz,\downarrow}, c_{\mathbf{k},zx,\uparrow}, c_{\mathbf{k},zx,\downarrow})^{\mathsf{T}}.$$

Furthermore, t and t' are σ- and π-bonding parameters of t_{2g} orbitals, respectively. Abbreviations for the momentum dependence are $c_{x(y)} = \cos k_{x(y)}$, $s_{x(y)} = \sin k_{x(y)}$. The lattice constant is taken to be unity. Terms proportional to γ in $\mathcal{H}_0$ mediate parity-violating hopping processes that can be cast as $\hat{z}\cdot(\mathbf{k}\times\mathbf{L})$ around the Γ point [11]. The energy difference

*hanjh@skku.edu

 ©2014 American Physical Society

TABLE I. Tight-binding parameters for STO and KTO. STO parameters are taken from Ref. [6]. KTO parameters are obtained from best fits to the graphs shown in Ref. [5]. Values are in units of eV.

	t	t'	δ	λ_{so}	γ
$SrTiO_3$	0.277	0.031	0.092	0.01	0.02
$KTaO_3$	0.75	0.075	1.0	0.15	0.01

between xy and yz (zx) orbitals is summed up as δ accounting for different responses of in-plane vs out-of-plane orbitals to surface confinement, surface crystal field, as well as lack of hopping terms in the z direction compared with the bulk system [5,6]. Numerical estimates of all tight-binding parameters extracted from Refs. [5,6] are summarized in Table I. Despite KTO having a much larger spin-orbit energy λ_{so} than STO, the overall surface band structures are qualitatively similar due to the even larger bandwidths set by t and t'.

Our strategy in investigating the linear and cubic Rashba effects in STO/KTO surfaces starts with a succession of two unitary rotations, given as

$$\mathcal{U}_1 = \begin{pmatrix} 1 & i\gamma k_x/\Delta & i\gamma k_y/\Delta \\ i\gamma k_x/\Delta & 1 & 0 \\ i\gamma k_y/\Delta & 0 & 1 \end{pmatrix}, \quad \mathcal{U}_2 = \begin{pmatrix} 1 & i\gamma' k_x^3/\Delta & i\gamma' k_y^3/\Delta \\ i\gamma' k_x^3/\Delta & 1 & 0 \\ i\gamma' k_y^3/\Delta & 0 & 1 \end{pmatrix}, \tag{2}$$

where

$$\Delta = t - t' - \delta/2 = E_{\rm gap}/2, \quad \gamma' = \gamma[(t-t')/2\Delta - 1/6].$$

When applied to $\mathcal{H}_0$ in Eq. (1), direct calculation shows $\mathcal{U} = \mathcal{U}_1\mathcal{U}_2$, around the Γ point,

$$\mathcal{U}^\dagger \mathcal{H}_0 \mathcal{U} \approx \begin{pmatrix} E^{(1)} & 0 & 0 \\ 0 & E^{(2)} & 0 \\ 0 & 0 & E^{(3)} \end{pmatrix},$$
$$E^{(1)} = -4t + \delta + t\left(k_x^2 + k_y^2 - \tfrac{1}{12}k_x^4 - \tfrac{1}{12}k_y^4\right),$$
$$E^{(2)} = -2t - 2t' + t\left(k_y^2 - \tfrac{1}{12}k_y^4\right) + t'\left(k_x^2 - \tfrac{1}{12}k_x^4\right),$$
$$E^{(3)} = -2t - 2t' + t\left(k_x^2 - \tfrac{1}{12}k_x^4\right) + t'\left(k_y^2 - \tfrac{1}{12}k_y^4\right). \tag{3}$$

Terms discarded in the diagonalization are at least fifth order in momentum $\mathbf{k}$, quite irrelevant for our discussion of cubic-order Rashba effects. We further assume small γ/Δ in order to guarantee unitarity of $\mathcal{U}_1$ and $\mathcal{U}_2$ up to order $(\gamma/\Delta)^2$. Since Δ is half the energy gap $E_{\rm gap}$ separating the lowest-energy d_{xy}-orbital-derived band from the other two at $\mathbf{k} = 0$, and reading of Table I gives $E_{\rm gap} \approx 0.4\ (0.35)$ eV for STO (KTO), the assumption is physically well justified.

Our method differs significantly in spirit from the early work of Winkler, who derived cubic Rashba terms specific to the strongly spin-orbit-coupled $J = 3/2$ and $J = 1/2$ bands [17]. Spin-orbit interaction (SOI) is not yet included at this stage; thus the results obtained will pertain to linear and cubic modulations of the OAM.

OAM averages of each band are given by the expectation values of $\mathbf{L} = (\sum_i \mathbf{L}_i)/N$, where $\mathbf{L}_i$ is the atomic OAM operator in the t_{2g}-orbital space at site i, and N is the number of lattice sites. It is convenient to separate the discussion for the lowest d_{xy}-orbital-dominated band (l band for short) from the other two, which are related to each other by a 90° spatial rotation. The calculated OAM for the l band is

$$L_+^{(l)} \approx -2i\frac{\gamma}{\Delta}k_+ + i\frac{\gamma}{\Delta}\left[\frac{1}{12} - \frac{t-t'}{4\Delta}\right]k_-^3, \tag{4}$$

where $L_\pm^{(l)} = \langle l,\mathbf{k}|(L_x \pm iL_y)|l,\mathbf{k}\rangle$ is the OAM average for the Bloch state of the l band at momentum $\mathbf{k}$, $k_\pm = k_x \pm ik_y$, and $\langle l,\mathbf{k}|L_z|l,\mathbf{k}\rangle = 0$. Note the cubic-order orbital winding k_-^3 having the opposite sense of "circulation" to the linear one, k_+.

Discussion of OAM for the upper two bands requires more care as energy values $E^{(2)}$ and $E^{(3)}$ become degenerate and switch their hierarchy at the diagonal lines $|k_x| = |k_y|$. It proves convenient to relabel the bands as $E^{(m)} = E^{(2)}$ for $|k_x| > |k_y|$ and $E^{(m)} = E^{(3)}$ for $|k_x| < |k_y|$, and the other way around for the upper band $E^{(u)}$. With $E^{(l)} < E^{(m)} \leqslant E^{(u)}$ in place over the whole Brillouin zone, we find

$$L_+^{(m)} \approx \begin{cases} P_y, & |k_x| > |k_y|, \\ P_x, & |k_x| < |k_y|, \\ 0, & |k_x| = |k_y|, \end{cases}$$
$$L_+^{(u)} \approx \begin{cases} P_x, & |k_x| > |k_y|, \\ P_y, & |k_x| < |k_y|, \\ P_x + P_y, & |k_x| = |k_y|, \end{cases} \tag{5}$$

where

$$P_x = i\frac{\gamma}{\Delta}(k_+ - k_-) + \frac{i}{2}\frac{\gamma}{\Delta}\left[\frac{1}{12} - \frac{t-t'}{4\Delta}\right](k_+^3 - k_-^3),$$
$$P_y = i\frac{\gamma}{\Delta}(k_+ + k_-) - \frac{i}{2}\frac{\gamma}{\Delta}\left[\frac{1}{12} - \frac{t-t'}{4\Delta}\right](k_+^3 + k_-^3).$$

As one can see clearly from Fig. 1, each quadrant displays nearly linear OAM patterns in either k_x or k_y directions within the two upper bands. Such quasilinear OAM patterns for the upper two bands of STO surface states is a strong, testable prediction readily measurable with the recently popular technique of circular dichroism ARPES [11,12,18].

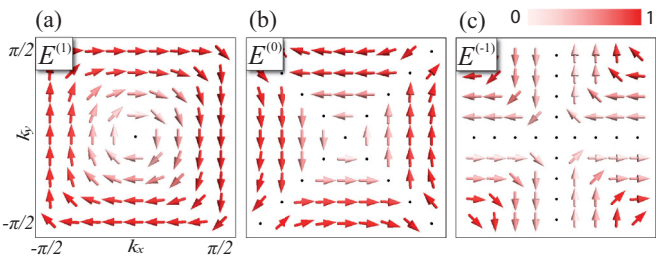

FIG. 1. (Color online) (a)–(c) OAM averages for the three bands obtained from numerical diagonalization of Eq. (1). Parameters are for STO (Table I) with $\lambda_{so} = 0$. Magnitude of OAM is represented on a false-color scale in units of $\hbar$. Directions and magnitudes of OAM vectors are consistent with Eq. (5).

III. DERIVATION OF CHIRAL SPIN ANGULAR MOMENTUM

Next step is to examine the influence of atomic spin-orbit interaction (SOI) $\mathcal{H}_{\rm so}$ on the orbital and concomitant spin polarizations. Although its influence is being considered after the ISB effects, the strength of SOI need not be smaller. The "diagonalization-by-unitary-rotation" procedure identifies the right set of basis states in the presence of ISB, wherein further interactions such as $\mathcal{H}_{\rm so}$ can be imposed. Spin-orbit Hamiltonian $H_{\rm so} = \lambda_{\rm so}\boldsymbol{\sigma}\cdot\mathbf{L}$ expressed in the unitary-transformed basis has matrix elements

$$\langle s,\sigma|\mathcal{H}_{\rm so}|s',\sigma'\rangle = \lambda_{\rm so}(\boldsymbol{\sigma})_{\sigma,\sigma'}\cdot(\mathcal{U}^{\dagger}\mathbf{L}\mathcal{U})_{s,s'}. \quad (6)$$

It means, in particular, that each 2×2 diagonal block of the spin-orbit matrix $\langle s,\sigma|\mathcal{H}_{\rm so}|s,\sigma'\rangle$ pertaining to the band index $s(=l,m,u)$, abbreviated $\mathcal{H}^{(s)}_{\rm so}$, is precisely

$$\mathcal{H}^{(s)}_{\rm so} = \lambda_{\rm so}[\sigma_+ L^{(s)}_- + \sigma_- L^{(s)}_+], \quad (7)$$

$\sigma^{\pm} = (\sigma^x \pm i\sigma^y)/2$, and $L^{(s)}_- = (L^{(s)}_+)^*$. Barring inter-band effects, it implies that spin Rashba splitting is a direct image of the corresponding momentum-space polarization of orbitals.

Symmetry consideration provides the basis to understand the nature of linear and cubic Rashba coupling. Interband effects are most negligible for the lowest-lying band separated from others by the gap $E_{\rm gap}$, permitting a reliable effective 2×2 Hamiltonian description. Such Hamiltonian $H^{(l)}_{\rm eff}$ constructed by the theory of invariants is, up to the third order in momentum $\mathbf{k}$,

$$H^{(l)}_{\rm eff} \approx \alpha^l_{\rm R}(k_x\sigma_y - k_y\sigma_x) + i\alpha^c_{\rm R}(k^3_+\sigma_+ - k^3_-\sigma_-). \quad (8)$$

Equation (7) for $s = l$ takes precisely this form dictated by symmetry, with parameters calculated from the microscopic approach. For the C_{3v}-symmetric surface of topological insulators, the cubic term in momentum $\mathbf{k}$ takes the form $\sim(k^3_+ + k^3_-)\sigma_z$ implying the out-of-plane spin polarization [14]. For C_{4v} symmetry of the perovskite surface the cubic term reads $\sim(k^3_+\sigma_+ + k^3_-\sigma_-)$, leading to in-plane spin structures. The two upper bands $s = m,u$ touch at $\mathbf{k} = 0$ with a nonnegligible interband matrix element arising from SOI.

IV. NUMERICAL RESULTS

Figure 2 describes band structures and OAM vectors on the Fermi surfaces in STO and KTO [5,7], obtained from full numerical diagonalization of Eq. (1). Although the band dispersions of STO and KTO surface states are qualitatively similar, the order-of-magnitude difference in their respective SOI strengths is clearly manifested in the orbital and spin angular momentum textures. In Fig. 2(b), directions and magnitudes of OAM vectors are nearly identical among each of the outer and inner spin-split subband pairs, indicating the OAM features predicted in Eq. (5) remain insensitive to nonzero SOI. Spin angular momentum (SAM), on the other hand, is fully polarized in opposite directions in each subband pair, either parallel or antiparallel to the underlying OAM. KTO, on the contrary, has outer and inner Rashba-split states with opposite relative orientations of both OAM and SAM vectors, as a consequence of the much stronger SOI strength. The maximum Rashba spin splitting along the Γ-X direction occurs around $|\mathbf{k}| \sim 0.44\pi$ (0.25π) with splitting energy $\Delta E_{\rm spin} \sim 20$ meV (28 meV) in STO (KTO). Despite the order-of-magnitude difference in SOI strengths, Rashba spin splittings in STO and KTO show comparable energy scales.

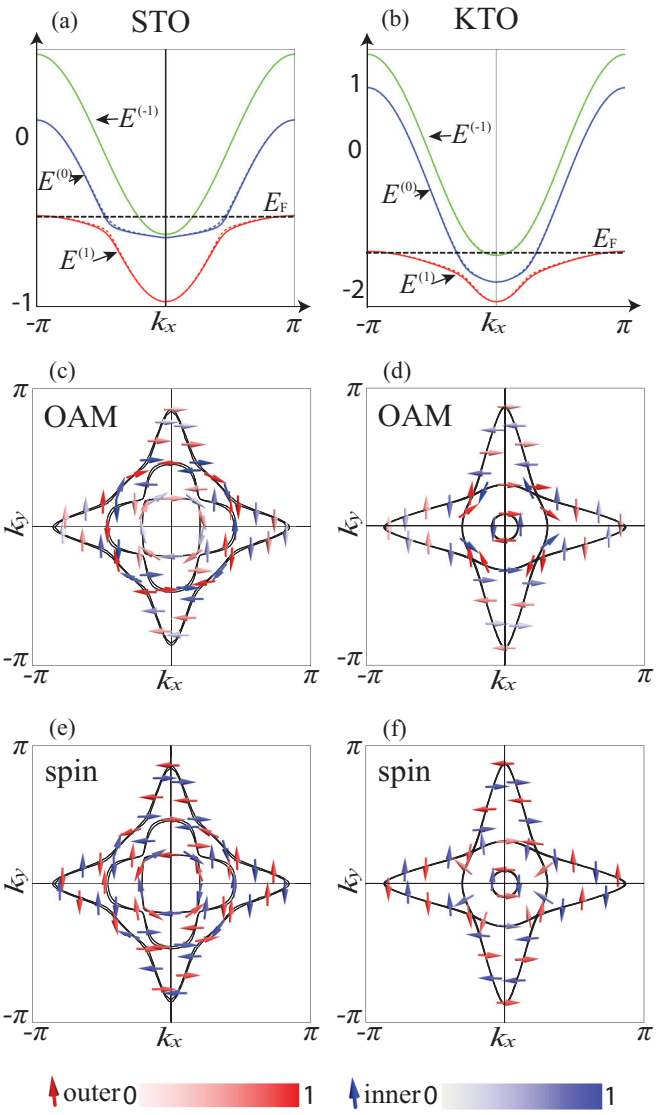

FIG. 2. (Color online) (a), (d) t_{2g}-band structures in STO and KTO obtained from respective tight-binding models. For each subband pair, outer (inner) band is denoted as solid (dotted) line. Energy on the y axis is in units of eV. (b), (e) Fermi surface at the energy $E_{\rm F}$ indicated in (a), (d) and corresponding OAM average vectors in STO and KTO. OAM averages of outer (inner) bands are represented as red (blue) arrows imposed on the Fermi surface contour. Directions of OAM vectors in outer and inner Rashba-split states are the same in STO [7], whereas those in KTO are opposite. (c), (f) Spin vectors on the Fermi surface in STO and KTO. Spin direction of outer (inner) band in STO is antiparallel (parallel) to that of OAM, whereas it is always antiparallel to OAM in KTO. Magnitude of OAM (spin) is represented on a false-color scale in units of $\hbar$ ($\hbar/2$).

Figure 3 illustrates the band-specific OAM and SAM vectors of KTO based on the first-principles calculation. Each

OAM/SAM structures obtained from density functional theory calculation [19] show excellent agreement with those from the numerical diagonalization of the tight-binding Hamiltonian.

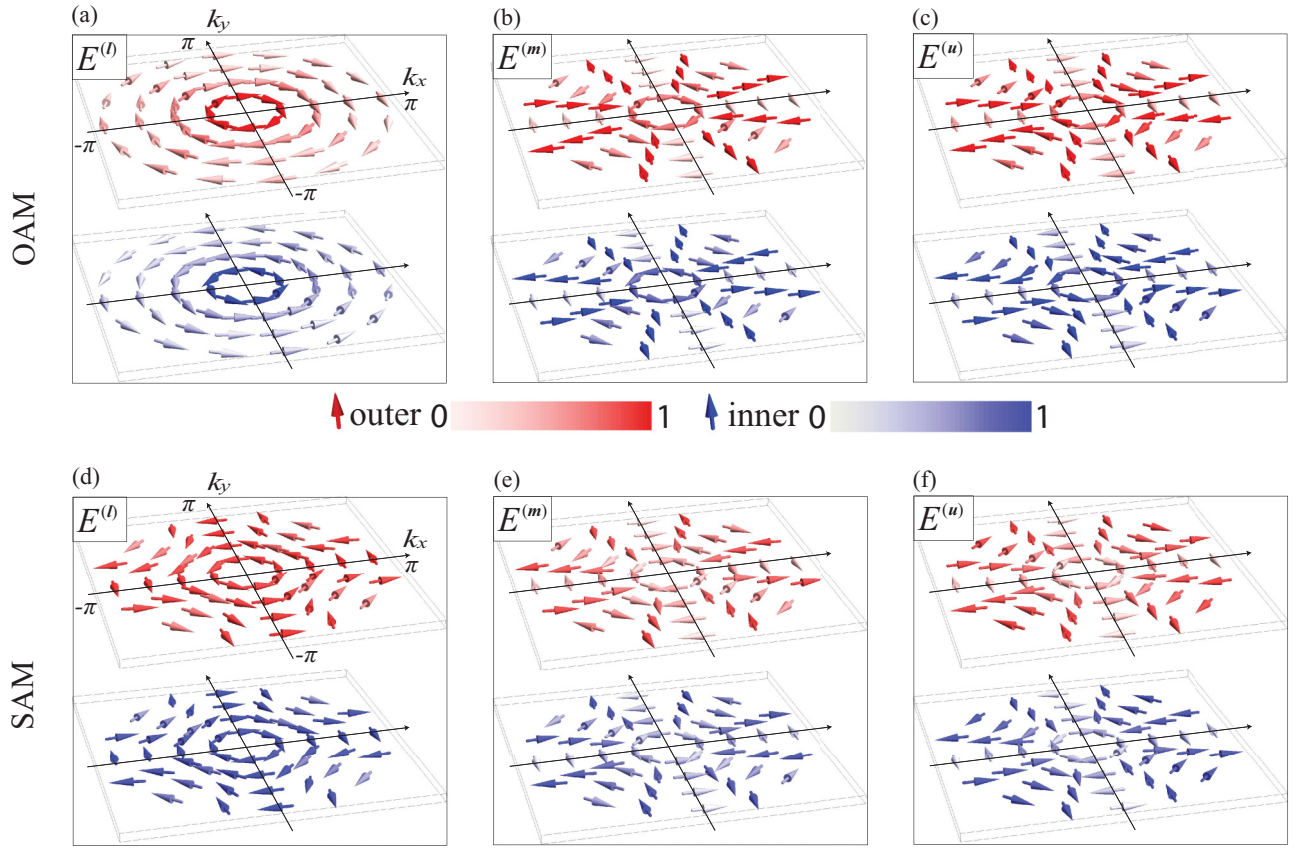

FIG. 3. (Color online) Band-specific (a)–(c) OAM vectors and (d)–(f) SAM vectors in KTO obtained from the first-principles calculation. In each figure, upper (lower) plot depicts the OAM or SAM structure of outer (inner) band. Each subband pair reveals opposite OAM and SAM direction for outer and inner bands. In addition to the rotating pattern around the Γ point in all the bands, a significant number of linear-polarized OAM and SAM vectors are present in the $E^{(m)}$ and $E^{(u)}$ bands. Magnitude of OAM (SAM) is represented on a false-color scale in units of $\hbar$ ($\hbar/2$).

subband pair has opposite OAM and SAM directions for outer and inner bands in the entire Brillouin zone.

V. DISCUSSION AND CONCLUSION

In this work we showed the lowest-lying surface bands of STO/KTO to be dominated by orbital and spin angular momentum chiralities of linear order in **k**, conventionally known as the orbital and spin Rashba effect. The upper two bands, according to our analytical, tight-binding, and density functional calculations, can at best be described as a complex mixture of linear and cubic terms in OAM/SAM structures, in contradiction to earlier claims of zero SAM/OAM for the middle band in the three-band surface system [10,11]. In fact in both Refs. [10,11] the authors have neglected the k^2 terms in the expansion of the energy dispersion around Γ before the inclusion of atomic SOI, which had the crucial effect of mixing only d_{xz} and d_{yz} orbitals in the band basis, leaving out the d_{xy} orbital entirely. The OAM average of the middle band in that case is automatically zero, implying the absence of linear spin Rashba effect as well. This assumption is however proven to be misleading by the present analysis as all three bands are shown to possess k-linear components of OAM and SAM vectors once the k^2 terms in the expansion are kept. The newly predicted OAM/SAM structures are also in much better accord with the results of density functional calculation. Regarding the transport measurement on the STO surface [8] supposedly in support of the cubic Rashba effect, we believe only a fresh calculation of the magnetotransport based on our improved understanding of the band and OAM/SAM structure can shed light on the implication of the data. We certainly do not believe the threefold angular dependence ($\sim\cos 3\theta$) in the magnetoresistance is a straightforward proof of the cubic Rashba effect.

Since the expected Rashba spin splitting is very small, the chances of its unambiguous detection with the current resolution of the ARPES setup are slim. The chiral structure of OAM, on the other hand, should be readily observable by means of circular dichroism ARPES [12,18]. The two would-be Rashba-split bands possess the same orbital chirality in STO, and therefore give rise to the same circular dichroism response. For KTO where the relative OAM directions cancel within the Rashba band pair, some other means of detecting their presence must be devised.

ACKNOWLEDGMENTS

P.K. acknowledges support from the Global Ph.D. Fellowship Program (NRF-2012). G.G. is supported by NRF Grant No. 2013R1A1A2058046. J.H.H. thanks the

LG Yonam Foundation for financial support and members of the condensed matter theory group at MIT for hospitality during the completion of this work. He is indebted to Andreas Santander-Syro for discussion of his experiments during the APCTP workshop "Bad Metal Behavior and Mott Quantum Criticality" in 2013.

[1] A. F. Santander-Syro, O. Copie, T. Kondo, F. Fortuna, S. Pailhès, R. Weht, X. G. Qiu, F. Bertran, A. Nicolaou, A. Taleb-Ibrahimi, P. Le Fèvre, G. Herranz, M. Bibes, N. Reyren, Y. Apertet, P. Lecoeur, A. Barthélémy, and M. J. Rozenberg, Nature (London) **469**, 189 (2011).

[2] W. Meevasana, P. D. C. King, R. H. He, S.-K. Mo, M. Hashimoto, A. Tamai, P. Songsiriritthigul, F. Baumberger, and Z.-X. Shen, Nat. Mater. **10**, 114 (2011).

[3] Pavlo Zubko, Stefano Gariglio, Marc Gabay, Philippe Ghosez, and Jean-Marc Triscone, Annu. Rev. Condens. Matter Phys. **2**, 141 (2011).

[4] P. D. C. King, R. H. He, T. Eknapakul, P. Buaphet, S.-K. Mo, Y. Kaneko, S. Harashima, Y. Hikita, M. S. Bahramy, C. Bell, Z. Hussain, Y. Tokura, Z.-X. Shen, H. Y. Hwang, F. Baumberger, and W. Meevasana, Phys. Rev. Lett. **108**, 117602 (2012).

[5] A. F. Santander-Syro, C. Bareille, F. Fortuna, O. Copie, M. Gabay, F. Bertran, A. Taleb-Ibrahimi, P. Le Fèvre, G. Herranz, N. Reyren, M. Bibes, A. Barthélémy, P. Lecoeur, J. Guevara, and M. J. Rozenberg, Phys. Rev. B **86**, 121107 (2012).

[6] Zhicheng Zhong, Anna Tóth, and Karsten Held, Phys. Rev. B **87**, 161102(R) (2013).

[7] P. D. C. King, S. McKeown Walker, A. Tamai, A. de la Torre, T. Eknapakul, P. Buaphet, S.-K. Mo, W. Meevasana, M. S. Bahramy, and F. Baumberger, Nat. Commun. **5**, 3414 (2014).

[8] H. Nakamura, T. Koga, and T. Kimura, Phys. Rev. Lett. **108**, 206601 (2012).

[9] Similar magnetoresistance measurement under the rotating direction of the magnetic field and analysis on KTO surface has yet to be carried out. See H. Nakamura and T. Kimura, Phys. Rev. B **80**, 121308 (2009).

[10] Y. Kim, R. M. Lutchyn, and C. Nayak, Phys. Rev. B **87**, 245121 (2013).

[11] Jin-Hong Park, Choong H. Kim, Jun-Won Rhim, and Jung Hoon Han, Phys. Rev. B **85**, 195401 (2012).

[12] Seung Ryong Park, Choong H. Kim, Jaejun Yu, Jung Hoon Han, and Changyoung Kim, Phys. Rev. Lett. **107**, 156803 (2011).

[13] Y. A. Bychkov and E. I. Rashba, JETP Lett. **39**, 78 (1984)

[14] Liang Fu, Phys. Rev. Lett. **103**, 266801 (2009).

[15] M. Onoda and N. Nagaosa, J. Phys. Soc. Jpn. **71**, 19 (2002).

[16] Jin-Hong Park, Choong H. Kim, Hyun-Woo Lee, and Jung Hoon Han, Phys. Rev. B **87**, 041301(R) (2013).

[17] R. Winkler, Phys. Rev. B **62**, 4245 (2000).

[18] Beomyoung Kim, Choong H. Kim, Panjin Kim, Wonsig Jung, Yeongkwan Kim, Yoonyoung Koh, Masashi Arita, Kenya Shimada, Hirofumi Namatame, Masaki Taniguchi, Jaejun Yu, and Changyoung Kim, Phys. Rev. B **85**, 195402 (2012).

[19] Density functional theory calculation is performed using the OPENMX code (http://www.openmx-square.org) within the local spin density approximation of Ceperly-Alder. The self-consistent norm-conserving pseudopotentials of K, Ta, and O were adopted from the OPENMX database.